

How to flatten a soccer ball

Kaie Kubjas, Pablo A. Parrilo and Bernd Sturmfels

Abstract This is an experimental case study in real algebraic geometry, aimed at computing the image of a semialgebraic subset of 3-space under a polynomial map into the plane. For general instances, the boundary of the image is given by two highly singular curves. We determine these curves and show how they demarcate the “flattened soccer ball”. We explore cylindrical algebraic decompositions, by working through concrete examples. Maps onto convex polygons and connections to convex optimization are also discussed.

1 Introduction

Computational tools for real algebraic geometry have numerous applications. This article offers a case study, focused on the following very simple scenario. We consider a compact semialgebraic subset of real 3-space that is defined by one polynomial h in three variables:

$$\mathcal{B} = \{ (u, v, w) \in \mathbb{R}^3 : h(u, v, w) \geq 0 \}. \quad (1)$$

We think of \mathcal{B} as our “soccer ball”. A *flattening* of \mathcal{B} is its image under a polynomial map

$$\phi : \mathbb{R}^3 \rightarrow \mathbb{R}^2, (u, v, w) \mapsto (f(u, v, w), g(u, v, w)). \quad (2)$$

Kaie Kubjas
Dept. of Mathematics and Systems Analysis, Aalto University, Finland, e-mail: kaie.kubjas@aalto.fi

Pablo A. Parrilo
Laboratory for Information and Decision Systems, Massachusetts Institute of Technology, Cambridge, USA, e-mail: parrilo@mit.edu

Bernd Sturmfels
Dept. of Mathematics, University of California, Berkeley, USA, e-mail: bernd@berkeley.edu

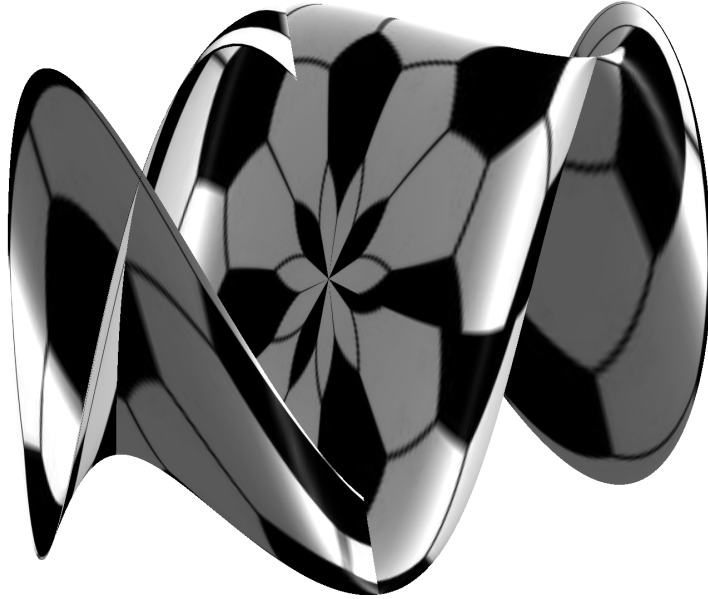


Fig. 1: A soccer ball is flattened and folded into a square.

Using quantifiers, the “flattened soccer ball” can be expressed as

$$\phi(\mathcal{B}) = \{(x, y) \in \mathbb{R}^2 : \exists u, v, w : x = f(u, v, w) \text{ and } y = g(u, v, w) \text{ and } h(u, v, w) \geq 0\}.$$

By Tarski’s theorem on quantifier elimination, the image is a semialgebraic set in the plane \mathbb{R}^2 , so it can be described as a Boolean combination of polynomial inequalities. Cylindrical algebraic decomposition [8] can be used to compute a quantifier-free representation. This is an active research area and several implementations are available [5, 7, 11, 14]. Our aim is to explore the main ingredients in such a representation of $\phi(\mathcal{B})$. A related problem is the computation of the convex hull $\text{conv}(\phi(\mathcal{B}))$, whose boundary points represent optimal points for the optimization problem of maximizing $\lambda f + \mu g$ over \mathcal{B} , where λ, μ are parameters.

This project started in November 2014 at the Simons Institute for the Theory of Computing in Berkeley, during the workshop *Symbolic and Numerical Methods for Tensors and Representation Theory*. The following example was part of its “Algebraic Fitness Session”.

Example 1. Consider the map given by the two elementary symmetric polynomials,

$$\phi : \mathbb{R}^3 \rightarrow \mathbb{R}^2, (u, v, w) \mapsto (uv + vw + uw, uvw).$$

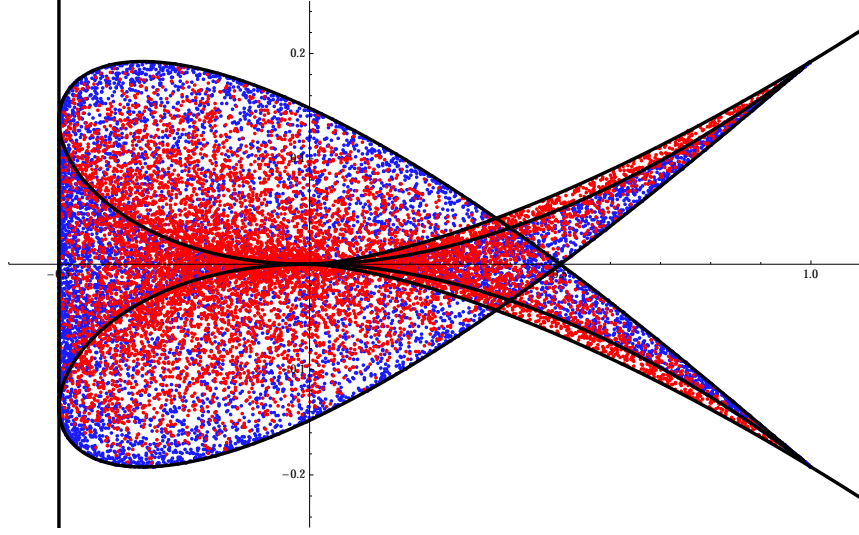


Fig. 2: Flattening of the unit ball \mathcal{B} under the map $(u, v, w) \mapsto (uv + vw + uw, uvw)$. Red points are randomly sampled from the interior of \mathcal{B} , and blue points are sampled from the boundary of \mathcal{B} .

We seek to compute the image under ϕ of the unit ball

$$\mathcal{B} = \{ (u, v, w) \in \mathbb{R}^3 : u^2 + v^2 + w^2 \leq 1 \}. \quad (3)$$

The flattened soccer ball $\phi(\mathcal{B})$ is the compact region in \mathbb{R}^2 that is depicted in Figure 2. In particular, $\phi(\mathcal{B})$ is not convex. If the second coordinate uvw were replaced by a homogeneous quadric then $\phi(\mathcal{B})$ would be convex, by a theorem of Brickman [6].

We can quickly get an impression of the flattened ball $\phi(\mathcal{B})$ by sampling points from the ball \mathcal{B} and plotting their images in \mathbb{R}^2 . These are the red points in Figure 2. We next sample points from the sphere $\partial\mathcal{B}$ and we plot these in blue. Figure 2 shows the existence of two small regions with many red points but no blue points at all. This means that the image of the sphere is strictly contained in the image of the ball. In symbols, $\phi(\partial\mathcal{B}) \subset \phi(\mathcal{B})$. The Zariski closure of the boundary of the image $\phi(\mathcal{B})$ is given by the polynomials

$$p = x^3 - 27y^2 \text{ and } q = (2x+1)(4x^6 - 4x^5 - 92x^3y^2 + x^4 + 6x^2y^2 + 729y^4 + 48xy^2 - 16y^2)$$

Here, p vanishes on the red boundary, while q vanishes on the blue boundary. \diamond

For a triple (f, g, h) of polynomials in $\mathbb{R}[u, v, w]$, representing the pair (\mathcal{B}, ϕ) , we define the *algebraic boundary* of $\phi(\mathcal{B})$ to be the Zariski closure in \mathbb{C}^2 of the topological boundary of $\phi(\mathcal{B})$. In addition to \mathcal{B} being compact, we also assume that \mathcal{B} is regular, i.e. the closure of the interior of \mathcal{B} contains \mathcal{B} . This excludes examples where lower-dimensional pieces stick out, like the Whitney umbrella. With these hy-

potheses, we can apply results in real algebraic geometry, found in [13, Lemma 3.1] and [19, Lemma 4.2], to conclude that the algebraic boundary is pure of dimension 1 in \mathbb{C}^2 . It is defined by the product of two squarefree polynomials p and q in $\mathbb{R}[x, y]$. The curve $V(p)$ is the branch locus of the map ϕ itself. It depends only on f and g but not on h . The curve $V(q)$ is the branch locus of the restriction of ϕ to the surface $V(h)$. It depends on h . Note that q is reducible in Example 1.

This paper is organized as follows. In Section 2 we study the algebraic geometry underlying our problem. If the data f, g, h are generic polynomials then the curves $V(p)$ and $V(q)$ are irreducible. We determine their Newton polygons and singularities. In Section 3 we explore the global topology of the flattened soccer ball $\phi(\mathcal{B})$. We present upper and lower bounds on the number of connected components in its complement. Section 4 introduces tools from symbolic computation for deriving an exact representation of $\phi(\mathcal{B})$. Section 5 offers connections to convexity and to sum-of-squares techniques in polynomial optimization.

2 Algebraic Curves

A standard approach in algebraic geometry is to focus on the generic instance in a family of problems. This then leads to an upper bound for the algebraic complexity of the output that is valid for all special instances. In what follows we pursue that standard approach.

Suppose that f, g and h are generic inhomogeneous polynomials of degrees d_1, d_2 and e in $\mathbb{R}[u, v, w]$. The soccer ball \mathcal{B} and the map ϕ are defined as in (1) and (2). Let p denote the squarefree polynomial that defines the branch locus of ϕ , and let q be the squarefree polynomial that defines the branch locus of $\phi_{\{h=0\}}$. These polynomials are unique up to scaling. They represent the algebraic boundary of $\phi(\mathcal{B})$. Both curves are in fact irreducible:

Theorem 1. *For generic polynomials f, g, h in $\mathbb{R}[u, v, w]$, the boundary polynomials p and q of the flattened soccer ball $\phi(\mathcal{B})$ are irreducible. Their Newton polygons are the triangles*

$$\begin{aligned} \text{Newt}(p) &= D_p \cdot \text{conv}\{(0, 0), (0, d_1), (d_2, 0)\} \text{ where } D_p = d_1^2 + d_1 d_2 + d_2^2 - 3d_1 - 3d_2 + 3; \\ \text{Newt}(q) &= D_q \cdot \text{conv}\{(0, 0), (0, d_1), (d_2, 0)\} \text{ where } D_q = e(d_1 + d_2 + e - 3). \end{aligned}$$

The irreducible complex curves $V(p)$ and $V(q)$ are highly singular, with genera

$$\begin{aligned} \text{genus}(p) &= \frac{1}{2}(2d_1^3 + 3d_1^2 d_2 + 3d_1 d_2^2 + 2d_2^3 - 13d_1^2 - 16d_1 d_2 - 13d_2^2 + 27d_1 + 27d_2 - 20), \\ \text{genus}(q) &= \frac{1}{2}(d_1^2 e + 2d_1 d_2 e + 3d_1 e^2 + d_2^2 e + 3d_2 e^2 + 2e^3 - 10d_1 e - 10d_2 e - 13e^2 + 21e + 2). \end{aligned}$$

The numbers of singular points of these curves in the complex affine plane \mathbb{C}^2 are

$$\begin{aligned} \#\text{Sing}(V(p)) &= \frac{1}{2}((D_p \cdot d_1 - 1)(D_p \cdot d_2 - 1) - D_p \cdot \gcd(d_1, d_2) + 1) - \text{genus}(p), \\ \#\text{Sing}(V(q)) &= \frac{1}{2}((D_q \cdot d_1 - 1)(D_q \cdot d_2 - 1) - D_q \cdot \gcd(d_1, d_2) + 1) - \text{genus}(q). \end{aligned}$$

In this statement, $\text{genus}(p)$ denotes the genus of the Riemann surface that is obtained by resolving the singularities of the curve $V(p)$. Equivalently, this is the *geometric genus*. The proof of Theorem 1 realizes the plane curves $V(p)$ and $V(q)$ as generic projections of smooth curves in 3-space. This implies that all their singular points are nodes (cf. [12]), and these are counted by the difference between the arithmetic genus and the geometric genus.

Table 1 underscores how singular our curves are. For instance, the last row concerns a general map ϕ of degree 4. The branch locus $V(q)$ of that map restricted to the boundary surface $V(h)$ has degree 56. A general plane curve of that same degree has genus 1485. However, the genus of our curve $V(q)$ is only 36, so it has $1485 - 36 = 1449$ singular points.

(d_1, d_2, e)	$\text{degree}(p)$	$\text{genus}(p)$	$\#\text{Sing}(V(p))$	$\text{degree}(q)$	$\text{genus}(q)$	$\#\text{Sing}(V(q))$
(1, 2, 2)	2	0	0	8	1	8
(1, 3, 2)	12	1	14	18	4	36
(2, 2, 2)	6	0	10	12	4	51
(2, 3, 2)	21	5	122	24	9	160
(2, 4, 2)	52	21	604	40	16	345
(3, 3, 2)	36	17	578	30	16	390
(3, 4, 2)	76	43	2048	48	25	792
(4, 4, 2)	108	82	5589	56	36	1449

Table 1: The numerical values in Theorem 1 for input polynomials of low degree.

From the polygon $\text{Newt}(p)$ in Theorem 1 we see that the curve $V(p)$ has degree $D_p \cdot \max(d_1, d_2)$, and similarly for $V(q)$. When the input polynomials f, g, h of degrees d_1, d_2, e are not generic but special, these numbers serve as an upper bound. We take the sum of these numbers to get

Corollary 1. *For any f, g, h , the algebraic boundary of $\phi(\mathcal{B})$ has degree at most*

$$(d_1^2 + d_1 d_2 + d_2^2 - 3d_1 - 3d_2 + 3 + e(d_1 + d_2 + e - 3)) \cdot \max(d_1, d_2).$$

This bound is tight when the polynomials f, g, h are generic relative to their degrees.

Remark 1. If $d_1 \leq d_2 = 2$ and e is arbitrary then the branch curve $V(p)$ of the map ϕ has genus 0. This means the curve admits a parametrization by rational functions.

The two cases given in the third and fourth row of Table 1 will be of most interest to us. For each of them, we may assume that \mathcal{B} is the unit ball (3), but ϕ is arbitrary.

Example 2. If we flatten the unit ball (3) via a quadratic map ($d_1 = d_2 = 2$) then the branch locus of ϕ is the rational sextic curve $V(p)$, with 10 singular points. The branch curve of the restriction of ϕ to $V(h)$ is the curve $V(q)$ of degree 12 and genus 4, so it has 51 singular points. These two curves make up the boundary of $\phi(\mathcal{B})$.

If both f and g are homogeneous quadrics then the image of \mathcal{B} under ϕ is convex. This follows from [6, Theorem 2.1]. More precisely, $\phi(\mathcal{B})$ is a spectrahedral shadow, bounded by a curve of degree six. This scenario corresponds to the case

$p = n = 3$ in Table 1 of [20]. The image $\phi(\mathcal{B})$ is generally not convex when one of the quadrics f, g is not homogeneous. For instance, the image of the unit ball under the map $(u, v) \mapsto (u^2 - v, v^2)$ is not convex. \diamond

Example 3. Let $d_1 = 2, d_2 = 3$ as in Example 1, but with f and g generic. The picture of $\phi(\mathcal{B})$ is now much more complicated than that in Figure 2. The red boundary $V(p)$ is a curve of degree 21 with 122 complex singular points, and the blue boundary $V(q)$ is a curve of degree 24 with 160 complex singular points. This is worked out in Example 8. \diamond

Proof (Proof of Theorem 1). We consider two curves in affine 3-space \mathbb{C}^3 . The curve C_1 is defined by the 2×2 -minors of the Jacobian matrix of (f, g) with respect to (u, v, w) . This 2×3 -matrix has general entries of degree $d_1 - 1$ in the first row and general entries of degree $d_2 - 1$ in the second row. By the Thom-Porteous-Giambelli Formula, we have $\deg(C_1) = (d_1 - 1)^2 + (d_1 - 1)(d_2 - 1) + (d_2 - 1)^2$. This expression equals D_p . The curve C_2 is the complete intersection defined by the polynomial h , which has degree e , and the Jacobian determinant of (f, g, h) with respect to (u, v, w) , which has degree $d_1 + d_2 + e - 3$. By Bézout's Theorem, $\deg(C_2) = e(d_1 + d_2 + e - 3)$. The hypothesis that f, g and h are generic ensure that C_1 and C_2 are smooth and irreducible. Their degrees are the quantities D_p and D_q in the statement.

Both of the results from algebraic geometry that were used in the previous paragraph (Thom-Porteous-Giambelli and Bézout) require certain genericity hypotheses on the geometric data to which they apply. These hypotheses are satisfied in our case because the given polynomials f, g and h are assumed to have generic coefficients. See e.g. [17, Section 3.5.4].

The curves defined by p and q are the images of C_1 and C_2 under the map $\phi = (f, g)$ from \mathbb{C}^3 to \mathbb{C}^2 . Our first claim states that, for $i = 1, 2$, the Newton polygon of the plane curve is the triangle $r \cdot \text{conv}\{(0, 0), (0, d_1), (d_2, 0)\}$, where $r = \deg(C_i)$.

We prove this using *tropical geometry* [15]. By genericity of f, g and h , the tropical curve $\text{trop}(C_i)$ in \mathbb{R}^3 is the 1-dimensional fan with rays spanned by $(1, 0, 0)$, $(0, 1, 0)$, $(0, 0, 1)$ and $(-1, -1, -1)$, where each ray has multiplicity r . Our goal is to compute the tropical curve $\text{trop}(\phi(C_i))$ in \mathbb{R}^2 . This contains the image of $\text{trop}(C_i)$ under the tropicalization of the map ϕ . This is the piecewise-linear map that takes (U, V, W) in \mathbb{R}^3 to $(\min\{d_1 U, d_1 V, d_1 W, 0\}, \min\{d_2 U, d_2 V, d_2 W, 0\})$. Its image is the weighted ray in \mathbb{R}^2 spanned by $(-d_1 r, -d_2 r)$. The other rays of the tropical curve $\text{trop}(\phi(C_i))$ arise from the points of C_i at which f and g vanish. We derive these using the method of Geometric Tropicalization, specifically [15, Theorem 6.5.11]. The relevant very affine curve is $C_i \setminus \{uvwfg = 0\}$, and the normal crossing boundary in the SNC pair is the divisor defined by $uvwfg$ on C_i .

The surface $\{f = 0\}$ meets the curve C_i in $d_1 r$ points, and the divisorial valuations at these points map to the weighted ray $(d_1 r, 0)$ in \mathbb{R}^2 . Likewise, the surface $\{g = 0\}$ meets C_i in $d_2 r$ points, and their divisorial valuations create the weighted ray $(0, d_2 r)$ in \mathbb{R}^2 . Hence the tropical plane curve $\text{trop}(\phi(C_i))$ consists of the three weighted rays specified by $(-d_1 r, -d_2 r)$, $(d_1 r, 0)$ and $(0, d_2 r)$. This implies our assertion about the Newton polygons of p and q .

To prove the second assertion, about the genera of the two curves in question, we use the following two facts about general curves in \mathbb{P}^3 . These are easily derived by computing the Hilbert series and then reading off the Hilbert polynomial. Recall that, for a curve with the Hilbert polynomial $h(n) = h_1n + h_0$, the degree is h_1 and the arithmetic genus is $1 - h_0$. Moreover, if the curve is smooth, then its geometric genus equals the arithmetic genus.

- A smooth space curve defined by the 2×2 -minors of a 2×3 -matrix with rows of degrees a and b has degree $a^2 + ab + b^2$ and genus $a^3 + \frac{3}{2}a^2b + \frac{3}{2}ab^2 + b^3 - 2a^2 - 2ab - 2b^2 + 1$.
- The complete intersection of two general surfaces of degrees a and b in \mathbb{P}^3 is a smooth curve of degree ab and genus $\frac{1}{2}ab(a + b - 4) + 1$.

The genus of the plane curve $V(p)$ is equal to the genus of the space curve C_1 that maps to it, and similarly for $V(q)$ and C_2 . So, it suffices to compute the genera of the affine curves C_1 and C_2 in \mathbb{C}^3 . We may work with their projective closures \bar{C}_1 and \bar{C}_2 in \mathbb{P}^3 . The curve \bar{C}_1 has the determinantal representation as in the first bullet, with $a = d_1 - 1$ and $b = d_2 - 1$. Substitution yields the desired formula for $\text{genus}(p)$. The curve \bar{C}_2 is the complete intersection of two surfaces in \mathbb{P}^3 , of degree $a = e$ and $b = d_1 + d_2 + e - 3$. Substituting these expressions into $\frac{1}{2}ab(a + b - 4) + 1$, we obtain the desired formula for $\text{genus}(q)$.

We can regard $V(p)$ and $V(q)$ as curves in the weighted projective plane given by the known Newton polygons. The genus of a general curve of the same degree is the number of interior lattice points on the Newton triangle. That number is equal to

$$\#(\mathbb{Z}^2 \cap \text{int}(\text{conv}\{(0,0), (0, rd_1), (rd_2, 0)\})) = \frac{1}{2}((rd_1 - 1)(rd_2 - 1) - \gcd(rd_1, rd_2) + 1).$$

Here r is D_p or D_q as before. The number of singular points is the number above minus the genus of the curve. This gives the count in the last assertion of Theorem 1.

We used the computer algebra system Macaulay2 [10] to verify some of the entries in Table 1. Here is the Macaulay2 code we used for a typical computation with $d_1 = d_2 = e = 2$:

```
S = QQ[x,y,u,v,w]; h = u^2+v^2+w^2-1;
f = u*v-u*w+7*v^2+v*w+5*w^2+u+v+w+1;
g = u^2-u*v+u*w-v^2+v*w-w^2+u-v+w-1;
C1 = minors(2, jacobian(ideal(f,g)));
C2 = minors(3, jacobian(ideal(f,g,h)))+ideal(h);
p = first first entries gens
      eliminate({u,v,w}, C1+ideal(x-f,y-g))
Ip = radical(ideal(diff(x,p), diff(y,p), p));
{degree p, # terms p, degree Ip}
q = first first entries gens
      eliminate({u,v,w}, C2+ideal(x-f,y-g))
Iq = radical(ideal(diff(x,q), diff(y,q), q));
{degree q, # terms q, degree Iq}
```

The polynomials p and q have degrees 6 and 12 respectively. The command `#terms` verifies that all monomials in the Newton polygons appear with non-zero coefficients. The singular loci of the two curves are given by their radical ideals, \mathbb{I}_p and \mathbb{I}_q . Applying the command `degree` to these ideals verifies that the number of singular points is 10 and 51 respectively.

3 Topological Complexity

When a soccer ball gets flattened, one generally expects the planar image to be simply connected. However, it is quite possible for $\phi(\mathcal{B})$ to have holes. In other words, the complement $\mathbb{R}^2 \setminus \phi(\mathcal{B})$ can have two or more connected components. In this section we present an explicit construction that makes this happen, with the number of holes being arbitrarily large.

The number of connected components of $\phi(\mathcal{B})$ is at most the number of connected components of \mathcal{B} . The number of its holes is counted by the first Betti number of $\phi(\mathcal{B})$. The best upper bounds for Betti numbers of compact semialgebraic sets are due to Basu and Riener [1, Theorem 10] and Basu and Rizzie [2, Theorem 27]. In our setting, the number of holes is bounded by $O(\max(d_1, d_2)^6 e^2)$ if $e \leq \max(d_1, d_2)$ and by $O(\max(d_1, d_2)^8)$ otherwise.

In what follows we assume that \mathcal{B} is the unit ball (3). The image $\phi(\mathcal{B})$ is a compact connected subset of \mathbb{R}^2 . We are interested in maps ϕ whose image $\phi(\mathcal{B})$ is not simply connected. The construction we shall give furnishes the lower bound $O(d_1 d_2)$ on the number of holes of $\phi(\mathcal{B})$. Based on *Lissajous curves*, it gives rise to some beautiful explicit examples.

The *Chebyshev polynomials (of the first kind)* are defined recursively by

$$T_0(t) = 1, T_1(t) = t \text{ and } T_{d+1}(t) = 2tT_d(t) - T_{d-1}(t) \text{ for } d \geq 1.$$

Explicitly, the Chebyshev polynomials are

$$T_2(t) = 2t^2 - 1, T_3(t) = 4t^3 - 3t, T_4(t) = 8t^4 - 8t^2 + 1, T_5(t) = 16t^5 - 20t^3 + 5t, \dots$$

They satisfy the trigonometric identity $\cos(d\theta) = T_d(\cos(\theta))$. Fix relatively prime positive integers d_1 and d_2 with $d_1 < d_2$. Let \mathcal{L}_{d_1, d_2} denote the Lissajous curve

$$x = \cos(d_1 \theta), y = \cos(d_2 \theta). \quad (4)$$

Its Zariski closure is the curve of degree d_2 with polynomial parametrization

$$x = T_{d_1}(t), y = T_{d_2}(t).$$

For instance, Lissajous curve $\mathcal{L}_{2,3}$ is the rational cubic $\{4x^3 - 2y^2 - 3x + 1 = 0\}$. It is singular at $(x, y) = (\frac{1}{2}, 0)$.

Example 4. Figure 3 shows the Lissajous curve $\mathcal{L}_{5,7}$. This curve has 12 singular points. This is the number of bounded regions in the complement of $\mathcal{L}_{5,7}$ in \mathbb{R}^2 .

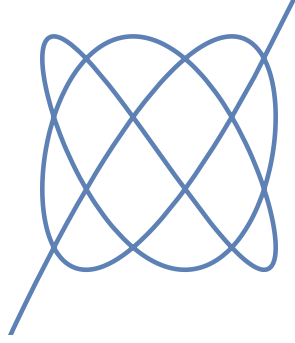


Fig. 3: The Lissajous curve $\mathcal{L}_{5,7}$.

Lemma 1. *The curve \mathcal{L}_{d_1,d_2} has precisely $\frac{(d_1-1)(d_2-1)}{2}$ complex singular points. All of these are real and are attained by two distinct values of θ in the trigonometric parametrization (4).*

Proof. By the same argument as in the proof of Theorem 1, the Newton polygon of the Lissajous curve \mathcal{L}_{d_1,d_2} is contained in the triangle with vertices $(0,0)$, $(d_2,0)$ and $(0,d_1)$. The number of interior lattice points of that triangle is $\frac{(d_1-1)(d_2-1)}{2}$. This is the genus of the generic curve with that Newton polygon. And, it hence is an upper bound on the number of complex singular points of the special curve \mathcal{L}_{d_1,d_2} .

We next exhibit $\frac{(d_1-1)(d_2-1)}{2}$ real singular points on \mathcal{L}_{d_1,d_2} that are in the image of (4). Pick any $k \in \{1, \dots, d_1 - 1\}$ and any $l \in \{1, \dots, d_2 - 1\}$. Consider the angles

$$\theta' = \pi\left(\frac{k}{d_1} + \frac{l}{d_2}\right) \quad \text{and} \quad \theta'' = \left|\pi\left(\frac{l}{d_2} - \frac{k}{d_1}\right)\right|. \quad (5)$$

If $\frac{l}{d_2} - \frac{k}{d_1} > 0$, then $\theta' - \theta'' = \frac{2k\pi}{d_1}$ and $\theta' + \theta'' = \frac{2l\pi}{d_2}$; otherwise $\theta' - \theta'' = \frac{2l\pi}{d_2}$ and $\theta' + \theta'' = \frac{2k\pi}{d_1}$. This means that θ' and θ'' map to the same point, and the Lissajous curve \mathcal{L}_{d_1,d_2} has a node at that point. There are $(d_1 - 1)(d_2 - 1)$ choices of pairs (k, l) . Since the trigonometric parametrization (4) is 2-to-1 on the interval $[0, 2\pi]$, this creates $\frac{(d_1-1)(d_2-1)}{2}$ nodal singularities on \mathcal{L}_{d_1,d_2} . This argument is a modification of [4, Section 2.1]. The lower bound we derived matches the upper bound in the previous paragraph, and this completes the proof.

We now apply this to flattening the soccer ball. Consider the map $\phi = (f, g)$ with

$$f(u, v, w) = T_{d_1}(u) + \varepsilon \cdot v, \quad g(u, v, w) = T_{d_2}(u) + \varepsilon \cdot w, \quad (6)$$

where $T_d(\cdot)$ is the degree- d Chebyshev polynomial, and $\varepsilon > 0$ is a small constant. The map ϕ takes the soccer ball \mathcal{B} and creates a two-dimensional image with many holes in \mathbb{R}^2 .

Example 5. Let $d_1 = 2$ and $d_2 = 3$. The set $\phi(\mathcal{B})$ is the region shown in Figure 4. It has precisely one hole. This picture was created by the following code in *Mathematica*, which produces a huge expression:

```
h = 1 - (u^2 + v^2 + w^2);
f = 2*u^2 - 1 + 1/10*v; g = 4*u^3 - 3*u + 1/10*w;
S = Exists[{u, v, w}, h >= 0 && x == f && y == g];
SR = Resolve[S, Reals]
RegionPlot[SR, {x, -1.2, 1.2}, {y, -1.2, 1.2}, PlotPoints -> 50]
```

The command “Resolve” performs quantifier elimination.

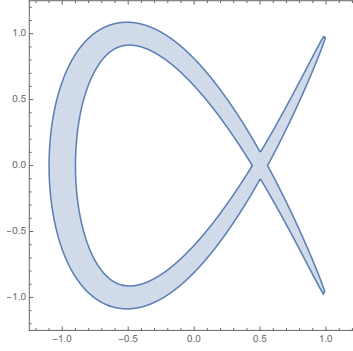


Fig. 4: The modification of the Lissajous curve in Example 5.

The following is our main result in this section.

Theorem 2. *Let $d_1 < d_2$ be relatively prime and ϕ as above with $\varepsilon > 0$ sufficiently small. Then, the complement of $\phi(\mathcal{B})$ in \mathbb{R}^2 has $\frac{(d_1-1)(d_2-1)}{2} + 1$ connected components. The algebraic boundary of $\phi(\mathcal{B})$ is an irreducible curve of degree at most $4d_2 - 2$. It is the branch locus of $\phi_{\{h=0\}}$, so it is defined by the polynomial that was denoted by q in Theorem 1.*

Proof. The part of the curve \mathcal{L}_{d_1, d_2} that lies in the square $[-1, 1]^2$ is compact. We regard this as an embedded planar graph, where the vertices are the nodal singularities given in (5) together with the two degree 1 endpoints, and the edges are the pieces of the Lissajous curve that connect the nodes and endpoints. This planar graph is 4-valent, the numbers of vertices, edges and faces satisfy $v - e + f = 2$ and $2e = 4(v - 2) + 2$. This implies $f = v - 1 = \frac{(d_1-1)(d_2-1)}{2} + 1$, i.e. the Lissajous curve has the correct number of holes.

As ε increases from 0 to being positive, the curve gets replaced by a two-dimensional region. But the number of holes in the complement does not change.

The algebraic boundary of $\phi(\mathcal{B})$ is given by the polynomials p and q that describe the branch curves of ϕ and $\phi_{\{h=0\}}$ respectively. However, in the present case, the curve $V(p)$ does not exist because the Jacobian of the map ϕ has rank 2 for all $(u, v, w) \in \mathbb{C}^3$. The Jacobian determinant of (f, g, h) with respect to (u, v, w) is the irreducible polynomial

$$\det \begin{pmatrix} \partial T_{d_1}/\partial u & \varepsilon & 0 \\ \partial T_{d_2}/\partial u & 0 & \varepsilon \\ -2u & -2v & -2w \end{pmatrix} = 2v\varepsilon \frac{\partial T_{d_1}}{\partial u} + 2w\varepsilon \frac{\partial T_{d_2}}{\partial u} - 2\varepsilon^2 u. \quad (7)$$

This is a polynomial of degree d_2 in which v and w occur linearly. The intersection of this surface with the unit sphere is an irreducible curve of degree at most $2d_2$. To compute the image of the curve, we substitute $v = \frac{1}{\varepsilon}(x - T_{d_1}(u))$ and $w = \frac{1}{\varepsilon}(y - T_{d_2}(u))$ into $h(u, v, w)$ and into (7). This results in two polynomials in u, x, y . Our task is to eliminate u . We do this by taking the determinant of the Sylvester matrix with respect to u . The non-constant entries in the Sylvester matrix have degree one or two in x or y . By examining their pattern in the matrix, we find that the determinant is a polynomial of degree at most $4d_2 - 2$.

Remark 2. We found experimentally that the Newton polygon of q is the triangle with vertices $(0, 0)$, $(4d_2 - 2, 0)$ and $(0, 2d_1 + 2d_2 - 2)$, but we could not prove this.

Example 6. We return to the flattened soccer ball seen in the introduction. To draw this picture from scratch in *Mathematica*, we run the code in Example 5, modified as follows:

```
f = u*v + v*w + u*w; g = u*v*w;
```

For this input, the output of the quantifier elimination command `Resolve` equals:

```
(-(1/2) <= x <= 0 && y == 0) ||
(y == -(1/(3*Sqrt[3])) && x == -(1/3)) ||
(-(1/(3*Sqrt[3])) < y < 0 &&
  Root[2*#1^3 + #1^2 - y^2 &, 1] <= x <=
  Root[2*#1^3 + #1^2 - y^2 &, 2]) ||
(y == 0 && Inequality[-(1/2), LessEqual, x, Less,
  0]) || (0 < y < 1/(3*Sqrt[3]) &&
  Root[2*#1^3 + #1^2 - y^2 &, 1] <= x <=
  Root[2*#1^3 + #1^2 - y^2 &, 2]) ||
(y == 1/(3*Sqrt[3]) && x == -(1/3)) ||
(x == -(1/2) && -(1/(3*Sqrt[6])) <= y <=
  1/(3*Sqrt[6])) || (-(1/2) < x < -(1/3) &&
  Root[729*#1^4 + #1^2*(-(92*x^3) + 6*x^2 + 48*x -
    16) + 4*x^6 - 4*x^5 + x^4 &, 1] <= y <=
  Root[729*#1^4 + #1^2*(-(92*x^3) + 6*x^2 + 48*x -
    16) + 4*x^6 - 4*x^5 + x^4 &, 4]) ||
(x == -(1/3) && -(1/(3*Sqrt[3])) <= y <=
  1/(3*Sqrt[3])) ||
(-(1/3) < x < (1/38)*(5*Sqrt[5] - 7) &&
  Root[729*#1^4 + #1^2*(-(92*x^3) + 6*x^2 + 48*x -
    16) + 4*x^6 - 4*x^5 + x^4 &, 1] <= y <=
```

```

Root[729*#1^4 + #1^2*(-(92*x^3) + 6*x^2 + 48*x -
16) + 4*x^6 - 4*x^5 + x^4 & , 4]] ||
(x == (1/38)*(5*Sqrt[5] - 7) && -Sqrt[2*x^3 + x^2] <=
y <= Sqrt[2*x^3 + x^2]) ||
((1/38)*(5*Sqrt[5] - 7) < x < 16/43 &&
Root[729*#1^4 + #1^2*(-(92*x^3) + 6*x^2 + 48*x -
16) + 4*x^6 - 4*x^5 + x^4 & , 1] <= y <=
Root[729*#1^4 + #1^2*(-(92*x^3) + 6*x^2 + 48*x -
16) + 4*x^6 - 4*x^5 + x^4 & , 4]] ||
(16/43 <= x <= 1/2 && -(Sqrt[x^3]/(3*Sqrt[3])) <=
y <= Sqrt[x^3]/(3*Sqrt[3])) ||
(1/2 < x < 1 && -(Sqrt[x^3]/(3*Sqrt[3])) <= y <=
Root[729*#1^4 + #1^2*(-(92*x^3) + 6*x^2 + 48*x -
16) + 4*x^6 - 4*x^5 + x^4 & , 2]] ||
Root[729*#1^4 + #1^2*(-(92*x^3) + 6*x^2 + 48*x -
16) + 4*x^6 - 4*x^5 + x^4 & , 3] <= y <=
Sqrt[x^3]/(3*Sqrt[3])) ||
(x == 1 && (y == -(1/(3*Sqrt[3])) ||
y == 1/(3*Sqrt[3])))

```

This is a quantifier-free formula for the flattened soccer ball in Figure 2. Most readers will find such an output hard to understand. The next section offers an alternative.

4 Exact Representation of the Image

Quantifier elimination for polynomial systems over \mathbb{R} is usually performed by cylindrical algebraic decomposition [8], abbreviated CAD. Many variants can be found in the recent literature, including *truth table invariant CAD* [5] and *variant quantifier elimination* [11]. CAD represents a semialgebraic set as a union of cells. In dimension one this would be a disjoint union of points and open intervals. Several implementations of CAD are now available, including QEPCAD [7], and the packages RegularChains [14] and ProjectionCAD [9] in Maple. In Example 6, we experimented with the implementation of CAD in Mathematica.

This section is purely expository, aimed at all mathematicians and their students. We show how to obtain a meaningful CAD “by hand” for all instances with parameters $d_1 = 2, d_2 = 3, e = 2$. Experts and CAD developers might find this useful as a family of test cases.

Consider the curve in \mathbb{R}^2 defined by the polynomial $p \cdot q$. Our image $\phi(\mathcal{B})$ is the closure of a union of connected components of its complement. We compute a partition of \mathbb{R}^2 that refines the partition given by $V(pq)$. A key step is to label each open piece in the finer partition. We then test which pieces lie in $\phi(\mathcal{B})$, and we report the labels of those that do.

Algorithm 1 describes what we do. The geometric idea is to project $V(pq)$ onto the x -axis. The critical points of that projection come in four flavors: singular points of $V(p)$, singular points of $V(q)$, points in the intersection $V(p, q)$, and smooth points on $V(pq)$ with vertical tangent lines. The *critical x -values* are the x -coordinates of all real critical points.

Algorithm 1 Quantifier-free representation of the flattened soccer ball $\phi(\mathcal{B})$

Input: Three polynomials $f, g, h \in \mathbb{Q}[u, v, w]$.

Step 1: Compute the polynomial p that defines the branch locus of the map ϕ .

Step 2: Compute the polynomial q that defines the branch locus of the restriction of ϕ to the boundary surface $V(h)$ of \mathcal{B} .

Step 3: Compute the sorted list C of all critical x -values of the polynomial $p \cdot q$.

Step 4: Sample points uniformly from \mathcal{B} and compute their images under the map ϕ . Save the result in a list S .

Step 5: For each $(\bar{x}, \bar{y}) \in S$ determine $k \in \mathbb{N}$ such that \bar{x} is between the k -th and $(k+1)$ -st element of C . Compute sorted list R of all real roots of the univariate polynomial $p(\bar{x}, y) \cdot q(\bar{x}, y)$. Determine $l \in \mathbb{N}$ such that \bar{y} is between the l -th and $(l+1)$ -st root in R .

Output: The polynomials p, q , the list C , and the set of all pairs (k, l) generated in Step 5.

Two consecutive critical x -values define a vertical strip. Here, the behavior of the curve segments does not change as x varies. In particular, curve segments do not cross or change direction. Curve segments pass from the left to the right over two consecutive critical x -values, and they divide the vertical strip into open regions. Two of them are unbounded and hence irrelevant. Each bounded region is either contained in $\phi(\mathcal{B})$ or is disjoint from $\phi(\mathcal{B})$.

Our description of $\phi(\mathcal{B})$ has three parts: the polynomials p and q that define the algebraic boundary, the critical x -values, and a set of pairs of positive integers. A pair (k, l) determines a region in \mathbb{R}^2 as follows. The x -coordinates are between the k -th and $(k+1)$ -st critical x -value, and the y -coordinates lie between l -th and $(l+1)$ -st curve segment in the y -direction.

Steps 1 and 2 of Algorithm 1 can be done with `Macaulay2`, as shown at the end of Section 2. Step 3 is more delicate because p and q are fairly large, even when f, g, h are small. The task is to compute the critical x -values of the polynomials p and q , and also the x -coordinates of the common zeros of p and q . To find these x -values symbolically, we compute three resultants of two polynomials in (x, y) with respect to y . Namely, we compute

$$\text{Res}_y(p, \partial p / \partial y), \text{Res}_y(q, \partial q / \partial y) \text{ and } \text{Res}_y(p, q). \quad (8)$$

At this stage one might compute the real roots of these three univariate polynomials in x . This can be done numerically using various methods, including the numerical algebraic geometry package in `Macaulay2`. However, we did not do this in our computations. Instead, we identify the real roots of our three resultants purely symbolically, using the command `Solve` with the option `Reals` in `Mathematica`. `Solve` tries to write each solution explicitly in terms of radicals, and if unsuccessful, it creates a representation as a root of a polynomial.

Since \mathcal{B} is compact, we can enclose it inside an appropriate cube in \mathbb{R}^3 . We sample points (u, v, w) with rational coordinates from that cube, and we throw out points that do not satisfy $h(u, v, w) \geq 0$. For instance, if \mathcal{B} is the unit sphere, then we first uniformly sample points from the cube $[-1, 1]^3$ and keep the points that satisfy $1 - u^2 - v^2 - w^2 \geq 0$.

Step 4 is probabilistic. As the number of samples grows to infinity, every region in the CAD of $\phi(\mathcal{B})$ will be reached and certified eventually. For any finite number of samples, there is a positive probability that some region is missed. Our approach can be turned this into a deterministic method by selecting a sample point in each region and deciding whether it has a preimage in \mathcal{B} . This amounts to testing whether a semialgebraic set in \mathbb{R}^3 is non-empty. The best known algorithm for deciding non-emptiness of a semialgebraic set is by Renegar [18]. In practice this can be done using implementations of CAD, but we decided not to pursue the deterministic variant in the present study.

In our examples we are also interested in deciding which regions of $\phi(\mathcal{B})$ lie in $\phi(\partial\mathcal{B})$. Note the distinction between the colors in Figure 2. For instance, to obtain points on the boundary of the unit ball, we uniformly sample points from the square $[-1, 1]^2$, keep the points that satisfy $1 - u^2 - v^2 \geq 0$, and create two boundary points with $w = \pm\sqrt{1 - u^2 - v^2}$.

In Step 5, we use binary search to determine k such that \bar{x} is between the k -th and $(k + 1)$ -st element of the list C . The symbolic representation derived in Mathematica is suitable for doing this. To be precise, we did the binary search with the following commands:

```
Block[{$ContextPath}, Needs["Combinatorica`"]]
k = Combinatorica`BinarySearch[C, x]-1/2
```

The real roots of $p(\bar{x}, y) \cdot q(\bar{x}, y)$ can again be computed using Mathematica command `Solve`. We now illustrate Algorithm 1 by applying it to the instance that launched this project.

Example 7. Fix f, g, h as in Example 1. The first part of the output are the polynomials p and q at the end of Example 1. The second part is the list of critical x -values:

$$-\frac{1}{2}, 0, \frac{16}{43}, \frac{2}{5}, \frac{1}{2}, 1. \quad (9)$$

The third part is a list which represents a partition of $\phi(\mathcal{B})$ into 22 regions:

$$(1, 1), (1, 2), (1, 3), (2, 1), (2, 2), (2, 3), (2, 4), (2, 5), (3, 1), (3, 2), (3, 3), \\ (3, 4), (3, 5), (4, 1), (4, 2), (4, 3), (4, 4), (4, 5), (5, 1), (5, 2), (5, 4), (5, 5).$$

The output above represents a quantifier-free formula for the flattened soccer ball. Using symbolic computation, we can assign one of the 22 labels to any sample point $\phi(u_0, v_0, w_0)$. For instance, $\phi(\mathcal{B}) \setminus \phi(\partial\mathcal{B})$ consists of the six regions $(3, 1), (3, 5), (4, 1), (4, 5), (5, 1), (5, 5)$.

From our output, we drew the picture in Figure 5. For this, we used the coordinates of all singular points and branch points of $V(pq)$. Branching occurs along the vertical tangent line $y = -\frac{1}{2}$. The real singular points are $(-\frac{1}{2}, -\frac{1}{3\sqrt{6}}), (-\frac{1}{2}, \frac{1}{3\sqrt{6}}), (0, 0), (\frac{16}{43}, -\frac{64}{129\sqrt{129}}), (\frac{16}{43}, \frac{64}{129\sqrt{129}}), (\frac{2}{5}, -\frac{2}{15\sqrt{15}}), (\frac{2}{5}, \frac{2}{15\sqrt{15}}), (\frac{1}{2}, 0), (1, -\frac{1}{3\sqrt{3}}), (1, \frac{1}{3\sqrt{3}})$. Four pairs of critical points have the same x -coordinates, seen in (9). The

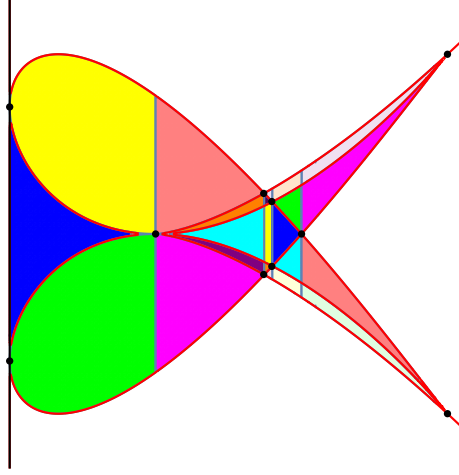


Fig. 5: The flattened soccer ball in Examples 1 and 7 is divided into 22 regions.

singular points and the vertical tangent line $y = -\frac{1}{2}$ are the black landmarks in Figure 5. The 22 regions are shown in different colors. The six regions in $\phi(\mathcal{B}) \setminus \phi(\partial\mathcal{B})$ are colored light.

The output of Algorithm 1 can be interpreted as a semialgebraic formula for $\phi(\mathcal{B})$, as follows: Consider $p \cdot q$ as a univariate polynomial in y . Write down its Sturm sequence. Let n denote the number of sign changes in that sequence evaluated at $-\infty$. The formula for the region (k, l) is a disjunction over all the possible sign assignments of the Sturm sequence with $n - l$ sign changes, in conjunction with x being between the k -th and $(k + 1)$ -st critical x -value. Such a formula will again be hard to read, just like the `Mathematica` output displayed at the end of Section 4. A description like Example 7, accompanied by a picture like Figure 5, seems to be the most human-friendly way to represent the result of flattening a soccer ball.

We next discuss a more serious example, where the `Resolve` command does not terminate. It will demonstrate the pros and cons of the exact symbolic approach.

Example 8. Fix $h = u^2 + v^2 + w^2 - 1$ as before, so \mathcal{B} is the unit ball. We select f and g randomly from polynomials of degree 2 and 3 respectively. This means we are now in the regime covered by Theorem 1. Note the fourth line in Table 1 marked $(d_1, d_2, e) = (2, 3, 2)$. The following instance, picked for us by `Macaulay2`, corresponds to the picture in Figure 6:

$$\begin{aligned} f &= \frac{3}{5}u^2 + uv + \frac{10}{3}v^2 + \frac{7}{3}uw + \frac{1}{4}vw + \frac{3}{10}w^2 + \frac{7}{4}u + \frac{8}{5}v + \frac{7}{5}w + \frac{10}{9}, \\ g &= \frac{1}{4}u^3 + 3u^2v + uv^2 + \frac{5}{3}v^3 + u^2w + \frac{8}{5}uvw + \frac{4}{7}v^2w + \frac{7}{3}uw^2 + \frac{7}{3}vw^2 + \frac{7}{10}w^3 + \\ &\quad \frac{7}{2}u^2 + 3uv + \frac{5}{9}v^2 + \frac{3}{8}uw + \frac{1}{9}vw + \frac{7}{4}w^2 + \frac{9}{2}u + \frac{3}{4}v + \frac{5}{6}w + \frac{3}{7}. \end{aligned}$$

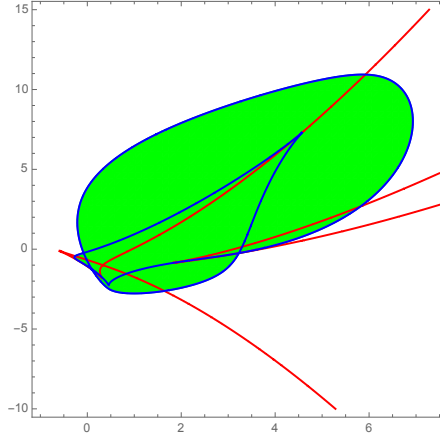


Fig. 6: The flattened soccer ball $\phi(\mathcal{B})$ in Example 8 and its algebraic boundary.

The polynomial p that describes the branch locus of ϕ has degree 21 and 169 terms. The polynomial q that describes the branch locus of $\phi_{\{h=0\}}$ has degree 24 and 217 terms. In both cases, these numbers count exactly the lattice points of the Newton triangles in Theorem 1.

For Step 3 we compute three univariate polynomials in x , namely the resultants in (8). The resultant of p and $\frac{\partial p}{\partial y}$ has degree 273 with 13 real roots. The resultant of p and $\frac{\partial q}{\partial y}$ has degree 360 with 22 real roots. The resultant of p and q has degree 336 with 16 real roots. All $13 + 22 + 16$ real roots are different, so the total number of critical x -values is 51. In Step 4 we sample points from the cube $[-1, 1]^3$ and from its boundary, and we record their images under ϕ . In Step 5, we run over these points in \mathbb{R}^2 , and we identify the labels (k, l) of the regions that contain these points. Some regions are very small. It takes a long time to identify them. We found that $\phi(\mathcal{B})$ is the union of the following 144 regions:

(12, 2), (13, 2), (13, 3), (14, 2), (14, 3), (14, 5), (15, 1), (15, 2), (15, 3), (15, 5), (16, 1), (16, 2),
 (16, 3), (16, 4), (16, 5), (17, 1), (17, 2), (17, 3), (17, 4), (17, 5), (18, 1), (18, 2), (18, 3), (18, 4),
 (18, 5), (19, 1), (19, 2), (19, 3), (19, 4), (19, 5), (20, 1), (20, 2), (20, 3), (20, 4), (20, 5), (20, 6),
 (20, 7), (21, 1), (21, 2), (21, 3), (21, 4), (21, 5), (21, 6), (21, 7), (22, 1), (22, 2), (22, 3), (22, 4),
 (22, 5), (23, 1), (23, 2), (23, 3), (23, 4), (23, 5), (24, 1), (24, 2), (24, 3), (24, 4), (24, 5), (24, 6),
 (24, 7), (25, 1), (25, 2), (25, 3), (25, 4), (25, 5), (26, 1), (26, 2), (26, 3), (26, 4), (26, 5), (27, 1),
 (27, 2), (27, 3), (27, 4), (27, 5), (28, 2), (28, 3), (28, 4), (28, 5), (29, 2), (29, 3), (29, 4), (29, 5),
 (29, 6), (29, 7), (30, 2), (30, 3), (30, 4), (30, 5), (30, 6), (30, 7), (31, 2), (31, 3), (31, 4), (31, 5),
 (31, 6), (31, 7), (32, 2), (32, 3), (32, 4), (32, 5), (32, 6), (32, 7), (33, 3), (33, 4), (33, 5), (33, 6),
 (33, 7), (34, 3), (34, 4), (34, 5), (34, 6), (34, 7), (35, 3), (35, 4), (35, 5), (35, 6), (35, 7), (36, 3),
 (36, 4), (36, 5), (36, 6), (36, 7), (37, 3), (37, 4), (37, 5), (37, 6), (37, 7), (38, 3), (38, 4), (38, 5),
 (38, 6), (38, 7), (39, 3), (39, 4), (39, 5), (40, 3), (40, 4), (40, 5), (41, 4), (41, 5), (42, 4), (43, 4).

Out of the 50 bounded segments between the critical x -values, precisely 32 arise from \mathcal{B} . The 11 left-most segments and the 7 right-most segments do not arise. In the list above, the first pair (12, 2) refers to x -coordinates between critical x -values labeled #12 and #13, which are approximately -0.275436 and -0.2599 . The corresponding y -coordinates are between the 2-nd and 3-rd root of $p \cdot q$, regarded as a polynomial in y , with x fixed in segment #12.

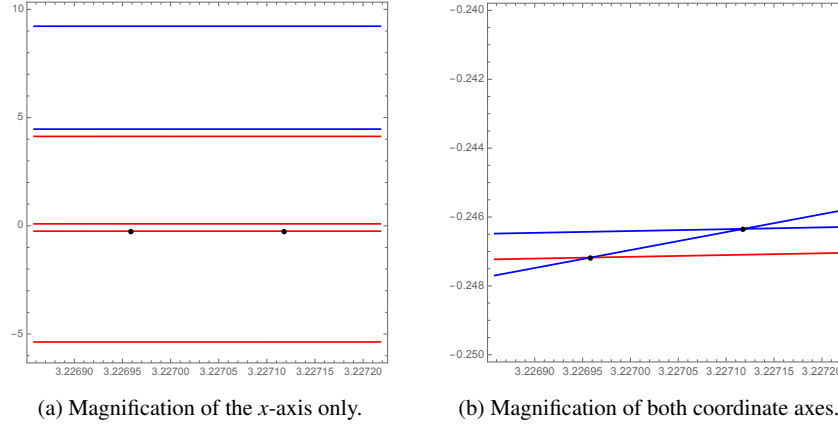


Fig. 7: Magnifications between the 33rd and 34th critical points.

Figure 7 shows that the situation is delicate. The regions can be very small, even for curves of degree 21. For example, consider the critical x -values labeled #33 and #34. They are 3.22696 and 3.22712. The unique critical point over #33 is an intersection point of $V(p)$ and $V(q)$. The unique critical point over #34 is a node of $V(q)$. They are shown in Figure 7.

In Figure 7a we scaled the x -axis so that it shows the vertical strip #33. The y -axis is left unscaled, so that we can see all curve segments in that strip. It looks like the blue curve $V(p)$ has two segments and the red curve $V(q)$ has four segments. However, two more blue segments are eclipsed by the relevant red segment. The truth becomes visible in Figure 7b, where we also scale the y -axis. The critical point on the right is a node of the blue curve $V(q)$ and it does not lie on the red curve $V(p)$. The left critical point lies in $V(p, q)$. Our careful analysis also shows that $\phi(\mathcal{B}) \neq \phi(\partial\mathcal{B})$, although this is not visible in Figure 6. Between critical x -values labeled #15 and #19, the lower boundary is given by the red curve $V(p)$.

5 Convexity and Optimization

The problem of computing images of maps is of considerable interest in polynomial optimization. Magron, Henrion and Lasserre [16] developed a method for this based

on outer approximations. Our study is complementary to theirs, in the sense that we do not consider approximations but we seek exact descriptions. A related question is how to compute and represent the convex hull of the image $\phi(\mathcal{B})$. This issue will be addressed later in this section.

We start our discussion with a few examples where both \mathcal{B} and $\phi(\mathcal{B})$ are convex. In what follows we retain the assumption that $h = u^2 + v^2 + w^2 = 1$, so \mathcal{B} is the unit ball in \mathbb{R}^3 . This can be folded into a convex polygon in various interesting ways.

Example 9. It is easy to find quadratic polynomials f and g such that $\phi = (f, g)$ maps the soccer ball onto a triangle or a rectangle. Figure 1 shows a map onto a square. Here are two explicit maps that work. If $f = u^2 + w^2$ and $g = v^2 + w^2$ then $\phi(\mathcal{B})$ is the square with vertices $(0, 0)$, $(0, 1)$, $(1, 0)$, $(1, 1)$, and $\phi(\partial\mathcal{B})$ is the triangle with vertices $(0, 1)$, $(1, 0)$, $(1, 1)$. The boundary polynomials are $p = xy(x - y)$ and $q = (1 - x)(1 - y)(x + y - 1)$. For a second example let ϕ be defined by $f = u^2 + 2v^2 + w^2 - 1$ and $g = u^2 + v^2 + 2w^2 - 1$. Now the flattened soccer ball $\phi(\mathcal{B})$ is the triangle with vertices $(-1, -1)$, $(0, 1)$, $(1, 0)$, while $\phi(\partial\mathcal{B})$ is the triangle with vertices $(0, 0)$, $(1, 0)$, $(0, 1)$. The difference $\phi(\mathcal{B}) \setminus \phi(\partial\mathcal{B})$ is not a convex set.

If we pass from quadratic maps to cubic maps then we can create other polygons.

Example 10. Use the cubic Chebyshev polynomial $T_3(t) = 4t^3 - 3t$ to define ϕ via

$$f(u, v, w) = \sqrt{3}(T_3(u) - T_3(v)) \quad \text{and} \quad g(u, v, w) = T_3(u) + T_3(v) - 2T_3(w).$$

The image $\phi(\mathcal{B})$ is the regular hexagon with vertices at $(0, \pm 4)$ and $(\pm 2\sqrt{3}, \pm 2)$.

This raises the question whether we can prescribe $\phi(\mathcal{B})$ to be any polyhedral shape. Ueno [21] proves that every unbounded convex polygon in \mathbb{R}^2 is the image of \mathbb{R}^2 under a polynomial map. It is not known, if his construction extends to polynomial images of the unit ball.

Problem 1. Let P be an arbitrary convex polygon in \mathbb{R}^2 . Construct explicit polynomials f and g in $\mathbb{R}[u, v, w]$ such that $P = \phi(\mathcal{B})$.

Our next topic is the *flattenings of pancakes*. These arise as special scenarios when we flatten soccer balls. Indeed, suppose that the map ϕ depends only on two of the variables, say

$$\phi : (u, v, w) \mapsto (f(u, v), g(u, v)).$$

Then the image of \mathcal{B} is the same as the image under $\phi' = (f, g)$ of the unit disk $\mathcal{D} = \{(u, v) \in \mathbb{R}^2 : u^2 + v^2 \leq 1\}$. In symbols, $\phi(\mathcal{B}) = \phi'(\mathcal{D})$. The unit disk \mathcal{D} serves the role of our *pancake*.

Example 11. Magron *et al.* [16, Example 1] illustrate their method for the map

$$f = \frac{1}{2}(u + uv) \quad \text{and} \quad g = \frac{1}{2}(v - u^3).$$

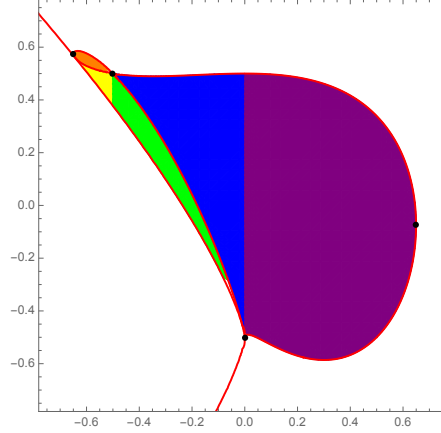


Fig. 8: This flattened pancake was discussed by Magron, Henrion and Lasserre [16].

It is instructive to compare their output with that of Algorithm 1. The exact description of the flattened pancake begins with the two polynomials that define the algebraic boundary:

$$\begin{aligned} p &= 2048x^3 + 432y^4 + 864y^3 + 648y^2 + 216y + 27, \\ q &= 64x^6 + 128x^5 + 96x^4 + 128x^3y - 32x^3 + 192x^2y^2 - 44x^2 \\ &\quad + 96xy^3 + 48xy^2 - 24xy - 12x + 16y^4 + 16y^3 - 4y - 1. \end{aligned}$$

The projection of the curve $V(pq)$ onto the x -axis has four critical points:

$$\left(-\frac{3\sqrt{3}}{8}, \frac{-473 + 264\sqrt{3}}{6208 - 3600\sqrt{3}}\right), \left(-\frac{1}{2}, \frac{1}{2}\right), \left(0, -\frac{1}{2}\right), \left(\frac{3\sqrt{3}}{8}, \frac{-473 - 264\sqrt{3}}{6208 + 3600\sqrt{3}}\right).$$

Our quantifier-free description of the planar region $\phi'(\mathcal{D})$ consists of the five pairs:

$$(1, 2), (1, 3), (2, 2), (2, 3), (3, 1).$$

Figure 8 shows $\phi'(\mathcal{D})$ where these five regions are colored in yellow, orange, green, blue and purple. The critical points are black, and the boundary curve $V(pq)$ is red.

Outer approximations of the kind studied in [16] tend to work best when one is interested not in the image itself but in its convex hull $\text{conv}(\phi(\mathcal{B}))$. Its extreme points are the solutions for the parametrized family of optimization problems

$$\gamma(\alpha, \beta) := \max\{\alpha x + \beta y : (x, y) \in \phi(\mathcal{B})\}. \quad (10)$$

The function γ is called the *support function* of the set $\phi(\mathcal{B})$. From the values of this function one obtains a description of the convex hull of $\phi(\mathcal{B})$ as an intersection of closed halfspaces:

$$\text{conv}(\phi(\mathcal{B})) = \bigcap_{(\alpha, \beta) \in \mathbb{R}^2} \{(x, y) : \alpha x + \beta y \leq \gamma(\alpha, \beta)\}.$$

The optimization problem in (10) can be equivalently written as

$$\gamma(\alpha, \beta) = \max_{(u, v, w)} \alpha f(u, v, w) + \beta g(u, v, w) \quad \text{s.t.} \quad h(u, v, w) \geq 0.$$

Both the objective function and the constraint are given by polynomial functions. Although in general this can be difficult to solve, good upper bounds can be obtained using *sum of squares* methods [3]. This method minimizes γ_{SOS} subject to

$$\gamma_{\text{SOS}} - (\alpha f(u, v, w) + \beta g(u, v, w)) = s_0(u, v, w) + s_1(u, v, w)h(u, v, w),$$

where s_0 and s_1 are *sums of squares*. The solution satisfies the inequality $\gamma \leq \gamma_{\text{SOS}}$. Furthermore, restricting the polynomials s_0, s_1 to have fixed degree, this is a semidefinite optimization problem, so it can be solved efficiently. Since $\gamma(\alpha, \beta) \leq \gamma_{\text{SOS}}(\alpha, \beta)$, we obtain an outer approximation of the convex hull:

$$\text{conv}(\phi(\mathcal{B})) \subseteq \bigcap_{(\alpha, \beta) \in \mathbb{R}^2} \{(x, y) : \alpha x + \beta y \leq \gamma_{\text{SOS}}(\alpha, \beta)\}. \quad (11)$$

The right hand side is a *spectrahedral shadow*, so it is a desirable set in the context of [3]. If one is lucky then equality holds in (11) and a semidefinite representation of $\text{conv}(\phi(\mathcal{B}))$ has been obtained. From our earlier algebraic perspective, such a representation still involves quantifiers. Any quantifier-free formula has to account for supporting lines that were created when passing from $\phi(\mathcal{B})$ to its convex hull. Those lines are bitangents of our curve $V(pq)$.

Acknowledgements Pablo Parrilo was supported by AFOSR FA9550-11-1-0305. Bernd Sturmfels was supported by NSF grant DMS-1419018 and the Einstein Foundation Berlin. Part of this work was done while the authors visited the Simons Institute for the Theory of Computing at UC Berkeley.

References

1. S. Basu and C. Riener: *Bounding the equivariant Betti numbers of symmetric semi-algebraic sets*, Advances in Mathematics **305** (2017), 803–855.
2. S. Basu and A. Rizzie: *Multi-degree bounds on the Betti numbers of real varieties and semi-algebraic sets and applications*, [arXiv:1507.03958](https://arxiv.org/abs/1507.03958).
3. G. Blekherman, P.A. Parrilo and R. Thomas: *Semidefinite optimization and convex algebraic geometry*, MOS-SIAM Series on Optimization **13**, SIAM, 2013.
4. M. Bogle, J. Hearst, V. Jones and L. Stoilov: *Lissajous knots*, J. Knot Theory Ramifications **3** (1994), 121–140.
5. R. Bradford, J. Davenport, M. England, S. McCallum and D. Wilson: *Truth table invariant cylindrical algebraic decomposition*, J. Symbolic Comput. **76** (2016), 1–35.

6. L. Brickman: *On the field of values of a matrix*, Proceedings of the American Mathematical Society **12** (1961), 61–66.
7. C.W. Brown: *QEPCAD B: A program for computing with semi-algebraic sets using CADs*, SIGSAM Bull. **37** (2003), 97–108.
8. G.E. Collins: *Quantifier elimination for real closed fields by cylindrical algebraic decomposition*, Springer Lecture Notes in Computer Science **33** (1975), 134–183.
9. M. England, D. Wilson, R. Bradford and J.H. Davenport: *Using the Regular Chains Library to build cylindrical algebraic decompositions by projecting and lifting*, in Mathematical Software – ICMS 2014, Springer, 2014.
10. D. Grayson and M. Stillman: *Macaulay2, a software system for research in algebraic geometry*, available at www.math.uiuc.edu/Macaulay2/.
11. H. Hong and M. Safey El Din: *Variant quantifier elimination*, J. Symbolic Comput. **47** (2012), 883–901.
12. T. Johnsen: *Plane projections of a smooth space curve*, in Parameter Spaces, 89–110, Banach Center Publications **36**, Polish Academy of Sciences, 1996.
13. T. Kahle, K. Kubjas, M. Kummer and Z. Rosen: *The geometry of rank-one tensor completion*, SIAM J. Appl. Algebra Geometry (2017).
14. F. Lemaire, M. Moreno Maza and Y. Xie: *The RegularChains library in MAPLE*, SIGSAM Bull. **39** (2005), 96–97.
15. D. Maclagan and B. Sturmfels: *Introduction to Tropical Geometry*, Graduate Studies in Mathematics **161**, American Mathematical Society, 2015.
16. V. Magron, D. Henrion and J.-B. Lasserre: *Semidefinite approximations of projections and polynomial images of semialgebraic sets*, SIAM J. Optim. **25** (2015), 2143–2164.
17. L. Manivel: *Symmetric Functions, Schubert Polynomials, and Degeneracy Loci*, SMF/AMS Texts and Monographs **6**, Cours Spécialisés **3**, American Mathematical Society, Société Mathématique de France, 2001.
18. J. Renegar: *On the computational complexity and geometry of the first-order theory of the reals*, J. Symb. Comput. **13** (1992), 255–352.
19. R. Sinn: *Algebraic boundaries of $SO(2)$ -orbitopes*, Discrete Comput. Geometry **50** (2013), 219–235.
20. R. Sinn and B. Sturmfels: *Generic spectrahedral shadows*, SIAM J. Optim. **25** (2015), 1209–1220.
21. C. Ueno: *On convex polygons and their complements as images of regular and polynomial maps of \mathbb{R}^2* , J. Pure Appl. Algebra **216** (2012), 2436–2448.